Experimental Cell Research 345 (2016) 37–50

Contents lists available at ScienceDirect

Experimental Cell Research

journal homepage: www.elsevier.com/locate/yexcr

Research Article

Inositol induces mesenchymal-epithelial reversion in breast cancer cells through cytoskeleton rearrangement

Simona Dinicola [a,b], Gianmarco Fabrizi [b,c], Maria Grazia Masiello [a,b], Sara Proietti [a,b], Alessandro Palombo [b,c], Mirko Minini [b,c], Abdel Halim Harrath [d], Saleh H. Alwasel [d], Giulia Ricci [e], Angela Catizone [f], Alessandra Cucina [b,g], Mariano Bizzarri [c,*]

[a] Department of Clinical and Molecular Medicine, Sapienza University of Rome, Viale Regina Elena 336, 00161 Rome, Italy
[b] Department of Surgery "Pietro Valdoni", Sapienza University of Rome, Via A. Scarpa 14, 00161 Rome, Italy
[c] Department of Experimental Medicine, Sapienza University of Rome, Systems Biology Group Lab, viale Regina Elena 324, 00161 Rome, Italy
[d] Department of Zoology, College of Science, King Saud University, PO Box 2455, 11451 Riyadh, Saudi Arabia
[e] Department of Experimental Medicine - Histology and Embryology Lab., Second University of Naples, Via Luciano Armanni 5, 80138 Naples, Italy
[f] Department of Anatomy, Histology, Forensic Medicine and Orthopedics - Section of Histology and Medical Embryology, Sapienza University of Rome, Via A. Scarpa 14/16, 00161 Rome, Italy
[g] Azienda Policlinico Umberto I, viale del Policlinico 155, 00161 Rome, Italy

ARTICLE INFO

Article history:
Received 16 November 2015
Received in revised form
10 May 2016
Accepted 10 May 2016
Available online 26 May 2016

Keywords:
Inositol
Cytoskeleton
EMT
MET
Invasion
Motility

ABSTRACT

Inositol displays multi-targeted effects on many biochemical pathways involved in epithelial-mesenchymal transition (EMT). As Akt activation is inhibited by inositol, we investigated if such effect could hamper EMT in MDA-MB-231 breast cancer cells. In cancer cells treated with pharmacological doses of inositol E-cadherin was increased, β-catenin was redistributed behind cell membrane, and metalloproteinase-9 was significantly reduced, while motility and invading capacity were severely inhibited. Those changes were associated with a significant down-regulation of PI3K/Akt activity, leading to a decrease in downstream signaling effectors: NF-kB, COX-2, and SNAI1. Inositol-mediated inhibition of PS1 leads to lowered Notch 1 release, thus contributing in decreasing SNAI1 levels. Overall, these data indicated that inositol inhibits the principal molecular pathway supporting EMT. Similar results were obtained in ZR-75, a highly metastatic breast cancer line. These findings are coupled with significant changes on cytoskeleton. Inositol slowed-down vimentin expression in cells placed behind the wound-healing edge and stabilized cortical F-actin. Moreover, lamellipodia and filopodia, two specific membrane extensions enabling cell migration and invasiveness, were no longer detectable after inositol addiction. Additionally, fascin and cofilin, two mandatory required components for F-actin assembling within cell protrusions, were highly reduced. These data suggest that inositol may induce an EMT reversion in breast cancer cells, suppressing motility and invasiveness through cytoskeleton modifications.

1. Introduction

Cell transitions from epithelial to mesenchymal (EMT), as well as from mesenchymal to epithelial phenotype (MET), play a pivotal role in organ and tissue remodeling, and they are also recognized as critical events which enable cancer cells in acquiring malignant features and metastatic competence [1]. Epithelial cancer cells, by acquiring mesenchymal-like characteristics, show reduced cell-cell adhesions and increased motility and invasiveness, which facilitate the escape of metastasis from the primary tumor [2]. EMT is thought to be critical not only for the transition leading from a low-malignant to an invasive carcinoma phenotype, but increasing evidence suggests that the EMT process is greatly associated with resistance to chemotherapy and radiotherapy [3,4].

These evidences prompted investigators to explore the mechanisms of EMT and methods to inhibit or even reverse this process and thereby inhibit tumor dissemination [5].

Induction of both EMT and MET may be triggered by both extracellular and intracellular cues, involving multiple molecular components which collectively lead to an in depth reorganization of the cytoskeleton. Some pathways seem to be critical for EMT, as those involving E-cadherin down-regulation, activation of TGFβ, Notch and Wnt-dependent processes, and SNAI1 overexpression [6]. These changes provide the molecular support required to dissolve epithelial cell-cell adhesions, to modify the interaction with the extra-cellular matrix (ECM), meanwhile cytoskeleton

* Corresponding author.
E-mail address: Mariano.bizzarri@uniroma1.it (M. Bizzarri).

http://dx.doi.org/10.1016/j.yexcr.2016.05.007
0014-4827/

components (actin, vimentin and tubulin) undergo profound reorganization. Remodeling of cell architecture eventually ends up in enabling cells acquiring enhanced migratory and invasive capabilities.

Compelling data indicate that such transformations are reversible, as they can be reversed by microenvironmental or molecular stimuli, and should therefore be viewed as adaptive modifications [7]. Focusing on MET processes, albeit challenging, is still likely to be an attractive approach to improve clinical management of cancer patients, especially for those at high risk of metastasis and recurrence. However, even if a number of putative targets have been identified, no reliable compounds for pharmacological use have been till now brought into being [8].

Inositol (INS) is a cyclohexane polyol, chemically represented by nine stereo isomeric compounds, among which myo-inositol is the most widely distributed in nature. INS can be synthesized by both prokaryotic and eukaryotic cells, even if in mammals it is mainly obtained from dietary sources, through hydrolysis of inositol-6-phosphate (phytic acid). Within the cells, INS is present in its free form, as inositol-mono, bi- and three-phosphate, or as phosphatidylinositol. Phosphatidylinositol can be further phosphorylated to form phosphatidylinositol phosphate and -biphosphate, which fulfill several relevant physiological roles [9]. Increasing evidence indicates that INS, by itself or through its derivatives, plays a relevant role in several critical biochemical pathway including morphogenesis, glucose metabolism, regulation of cell proliferation and fertility [10–12]. Moreover, a few even promising reports highlighted that INS may significantly inhibit development and progression of several cancer types, by modulating a wide array of biochemical cues [13].

Yet, some studies provided intriguing insights about INS-related effects on cytoskeleton, showing that inositol-monophosphate- and -biphosphate, induce actin synthesis [14], and F-actin ring formation at cell-cell contacts through Rock-dependent myosin II activation [15].

Herein we investigated if INS, as myo-inositol, may effectively interfere with cytoskeleton architecture in malignant MDA-MB-231 breast cancer cells in which several mesenchymal features have been recognized, and how this hypothesized effect could be associated to changes in the expression of key-molecular parameters, eventually triggering a mesenchymal-epithelial transition. To confirm these results, key-signaling pathways were investigated on one more highly metastatic cancer cell line (ZR-75).

2. Material and methods

2.1. Experimental cell model and inositol treatment

The human breast cancer cell lines MDA-MB-231 and ZR-75 were obtained from European Collection of Cell Cultures (ECACC). Cells were seeded into 25-cm^2 flasks (Falcon, Becton–Dickinson Labware, Franklin Lakes, NJ, USA) in DMEM supplemented with 10% Fetal Calf Serum (FCS) and antibiotics (Penicillin 100 IU/ml, Streptomycin 100 μg/ml, Gentamycin 200 μg/ml). The cultures were kept at 37 °C in an atmosphere of 5% CO_2 in air, and the medium was changed every third day. At confluence, the cells were sub-cultured after removal with 0.05% trypsin–0.01% EDTA.

Inositol was kindly provided by Lo. Li. Pharma s.r. L., Roma, Italy (myo-inositol ANDROSITOL® LAB). Inositol was added at the pharmacological concentration of 4 mM. Also, key molecular parameters were investigated by adding inositol at a physiological concentration (0.1 mM). At both 4 and 0.1 mM, inositol did not induce modifications in proliferation neither cell death (data not shown).

2.2. Western blot

MDA-MB-231 and ZR-75 human breast cancer cells were incubated with 4 mM INS for 24 h. Moreover, MDA-MB-231 cancer cells were incubated with 0.1 mM INS for 24 and 72 h. Untreated cells represented the control conditions. Following the treatment, the cells were washed twice with ice-cold PBS and scraped in RIPA buffer (Sigma Chemical Co., St Louis, MO, USA). A mix of protease inhibitors (Complete Mini Protease Inhibitor Cocktail Tablets, Roche, Mannheim, Germany) was added just before use. Cellular extracts were then centrifuged at 8000 g for 10 min. The protein content of supernatants was determined by using the Bradford assay.

For western blot experiments, cellular extracts were separated on a 12% SDS–polyacrylamide gel. Proteins were blotted onto nitrocellulose membranes (BIO-RAD, Bio-Rad Laboratories, Hercules, CA, USA) and probed with the following antibodies: PI3K (sc-1637, Santa Cruz Biotechnology), p-Akt (#9271, Cell Signaling Technology), Akt (#9272, Cell Signaling Technology), COX-2 (sc-19999, Santa Cruz Biotechnology), Snai1 (#3879, Cell Signaling Technology), α-SMA (ab5694, Abcam), Rock-1 (sc-5560, Santa Cruz Biotechnology), Rock-2 (sc-5561, Santa Cruz Biotechnology), PS1 (#MAB5232, Millipore), Notch 1 (sc-373891, Santa Cruz Biotechnology), cofilin (sc-33779, Santa Cruz Biotechnology), p-MYL9 (sc-12896, Santa Cruz Biotechnology), E-cadherin (sc-7870, Santa Cruz Biotechnology), β-catenin (sc-7963, Santa Cruz Biotechnology), fascin (sc-28265, Santa Cruz Biotechnology), NF-κB (sc-109, Santa Cruz Biotechnology) and GAPDH (#2118, Cell Signaling Technology). Antigens were detected with an enhanced chemoluminescence (ECL) kit from Amersham (Amersham Biosciences, Little Chalfont, Backinghamshire, England) according to the manufacturer's instructions. For each data point, three independent experiments were performed.

2.3. Densitometry

All western-blot images were acquired and analyzed through Imaging Fluor S densitometer (Biorad-Hercules). Optical density (OD) of each condition was normalized *versus* the signal of internal control GAPDH.

2.4. Wound healing assay

The Wound Healing Assay was performed using special double well culture inserts (ibidi GmbH, Am Klopferspitz 19, D-82152 Martinsried, Germany). Each insert was placed in a well of a 6-well plate (Falcon; Becton Dickinson Labware, Franklin Lakes, NJ, USA). We use three insert for each condition (CTRL and INS-treated cells) and 70 μl of each cell suspension (prepared at the concentration of 5×10^5 cells/ml) were placed into both well of each insert. After cells attachment, the culture inserts were gently removed and control cells were fed with DMEM 10% FBS meanwhile treated cells with DMEM 10% FBS and 4 mM INS. Plates were then incubated at 37 °C in an atmosphere of 5% CO_2 and cells were photographed at 10X magnification with a Nikon DS-Fi1 (Nikon Corporation, Japan) camera, coupled with a Zeiss.

Axiovert 10 optical microscope, at 0, 6, 10 and 12 h. Images were then analyzed with TScratch software (Copyright 2008, Tobias Gebäck and Martin Schulz, ETH Zürich, www.cse-lab.ethz.ch).

2.5. Cell migration assay

MDA-MB-231 cells (5×10^3 cells/200 μl medium) were placed in the upper side of 8-μm filters (Falcon, BD Biosciences) (upper chamber), placed in wells of a 24-well plate (Falcon, BD Biosciences) (lower chamber), containing 0.8 ml of medium. After 24 h

of starvation, 200 μl of DMEM 1% FBS was added into the upper chamber, while the lower chamber contained DMEM 10% FBS (0.8 ml) for untreated cells and DMEM 10% FBS with 4 mM INS. Chambers were kept in an incubator for 24 h. After incubation, cells from the upper surface of filters were removed with gentle swabbing, and the migratory cells on the lower surface of membranes were fixed and stained with haematoxylin/eosin. The membranes were examined microscopically, and cellular migration was determined by counting the number of cells on membranes in at least 4–5 randomly selected fields using a Zeiss Axiovert 10 optical microscope. For each data point, four independent experiments in duplicate were performed.

2.6. Cell invasion assay

The ability of MDA-MB-231 human breast cancer cells for passing through Matrigel-coated 8-μm filters (BD Bio-CoatTM growth factor reduced MATRIGELTM invasion chamber, BD Biosciences-Discovery Labware, Two Oak Park, Bedford, MA, USA) was measured by the Boyden chamber invasion assay. In brief, cells were treated with 4 mM INS. After 24 h, cells were detached by trypsin and resuspended in serum-free medium. Medium containing 10% FCS for untreated cells and DMEM 10% FCS with 10 μM INS for treated cells was applied to the lower chamber as chemoattractant, and then, the cells were seeded on the upper chamber at a density of 5×10^3 cells/well in a 200 μl of serum-free medium. The chamber was incubated for 24 h at 37 °C. At the end of incubation, the cells in the upper surface of the membrane were carefully removed with a cotton swab, and cells invaded across the Matrigel to the lower surface of the membrane were fixed with methanol and stained with haematoxylin and eosin. The invasive cells on the lower surface of the membrane filter were counted with Zeiss Axiovert 10 optical microscope. For each data point, three independent experiments in duplicate were performed.

2.7. MMPs gelatin zymography

The enzymatic activities of MMP-2 and MMP-9 were determined by gelatin zymography. Briefly, conditioned media of MDA-MB-231 human breast cancer untreated control cells and 4 mM INS treated cells were prepared with standard SDS–polyacrylamide gel loading buffer containing 0.01% SDS without β-mercaptoethanol and not boiled before loading. Then, prepared samples were subjected to electrophoresis with 12% SDS–PAGE containing 1% gelatin.

After electrophoresis, gels were washed twice with distilled water containing 2.5% Triton-X100 for 30 min at room temperature to remove SDS and then incubated in collagenase buffer (0.5 MTris-HCl pH 7.5, 50 mM $CaCl_2$ and 2 M NaCl) overnight at 37 °C, stained with Coomassie brilliant blue R-250 and destained with destaining solution (30% methanol, 10% acetic acid, and 60% water). MMP gelatin zimography was performed three times.

2.8. Confocal microscopy

Untreated control cells and 4 mM INS treated MDA-MB-231 human breast cancer cells were cultured into 8-well μ-slides (ibidi GmbH, Am Klopferspitz 19, D-82152 Martinsried, Germany) for 24 h. Then, the cells were fixed with 4% paraformaldehyde for 10 min at 4 °C and washed twice for 10 min with PBS. The cells were permeabilized for 30 min using PBS, 3% BSA, 0.1% Triton X-100, followed by the anti-β-catenin antibody (sc-7963, Santa Cruz Biotechnology), anti-N-cadherin (sc-7939, Santa Cruz Biotechnology), anti-fascin (sc-28265, Santa Cruz Biotechnology), anti-vimentin (sc-6260, Santa Cruz Biotechnology) staining in PBS, 3% BSA at 4 °C overnight. The cells were washed with PBS and incubated for 1 h at room temperature with TRITC fluorophore–conjugated secondary donkey anti-mouse antibody (Invitrogen Molecular Probes Eugene, Oregon). The slides were then washed with PBS and mounted with 0.1 mM Tris-HCl at pH 9.5: glycerol (2:3). Negative controls were processed in the same conditions besides primary antibody staining. For F-actin visualization Rhodamine Phalloidin (Invitrogen Molecular Probes Eugene, 1: 40 dilution) was used. Cells were fixed in 4% paraformaldehyde (PFA) in PBS for 10 min at 4 °C and then permeabilized with cold ethanol: Acetone 1: 1 for 10 min at 4 °C. After rinsing, cells were incubated with Rhodamine Phalloidin for 25 min in the dark. Cells were then washed in PBS and mounted in buffered glycerol (0.1 M, pH 9.5). TOPRO-3 labeling was used for nuclei. Finally, analysis was conducted using a Leica confocal microscope (Laser Scanning TCS SP2) equipped with Ar/ArKr and He/Ne lasers. Laser lines were at 488, 543 and 633 nm for FITC, TRITC and TOPRO-3 excitation respectively. The images were scanned under a 20x objective or 40x oil immersion objective. In order to get a quantitative analysis of fluorescence, optical spatial series with a step size of 1 μm, were performed both in untreated and in INS-treated samples. The fluorescence intensity was determined by the Leica confocal software, using the following parameters: the maximum amplitude of fluorescence (MAX Amplitude), the sum of intensity (SUM (I)), of positive areas. As we previously reported [16] the MAX Amplitude represents the maximum intensity of fluorescence of each series. The SUM (I) represents the total amount of fluorescence intensity recovered within the entire section. We analyzed equivalent sized regions of interest (ROI) for each experiment both in untreated and in INS-treated samples.

2.9. Image analysis

For MDA-MB-231 cell line, image analysis was performed on 544 control cells and on 606 treated cells (with 4 mM INS for 24 h), randomly chosen from 20 images. Cells were contoured with a fine black marker by different researchers, simply scanned and processed to evaluate quantitative parameters (area A, solidity and roundness), as previously described [17]. Briefly, all images were processed by Adobe Photoshop CS4 and pictures were resized at 2560×1920 pixels according to original scale of image acquisition. For each black contoured cell, edges were refined. Then cells were black filled and threshold was adjusted in order to exclude from the image other cells and background. For each cell group, a single sheet of all the cells considered was created. To obtain single cell shape parameters ImageJ v 1.47 h software was used. Then, the software analyzed single cells, by the function "shape descriptor." In addition to area A, parameters were quantified according to the following formulas:

$$Solidity = \frac{A}{CA}$$

$$Roundness = \frac{4A}{\pi\sqrt{ma}}$$

where A is the area of the cell, ma is the major axis, and CA is the convex area, namely the area of the convex hull of the region. The convex hull of a region is the smallest region that satisfies two conditions: (a) it is convex (b) it contains the original region.

2.10. Coherency quantification as cytoskeleton quantitative measure

Images from untreated control and from 4 mM INS treated MDA-MB-231 cancer cells (8 images for each condition) were considered, and 40 cells were randomly chosen, respectively for the control and the INS treated samples. We analyzed by means of ImageJ v 1.47 h software equivalent sized regions of interest (ROI)

for each experimental condition.

Images were then processed in order to exclude the background. As quantitative parameter indicating cytoskeleton rearrangement, coherency was measured as previously described [18]. Calculation was made by using the plugin OrientationJ [19].

2.11. Statistical analysis

Results were expressed as mean ± SD, and statistical analysis was performed through unpaired, two-tailed Student's *t* test. Vimentin quantitative distribution was expressed as mean ± SE, and statistical analysis was performed through unpaired, two-tailed Student's *t* test. Differences were considered significant at the level of $p < 0.05$. Statistical analysis was performed using GraphPad Instat software (GraphPad Software, Inc.; San Diego, CA, USA).

3. Results

3.1. Inositol inhibits PI3K/Akt pathway

PI3K pathway activation is an early event in carcinogenesis [20]. Phosphoinositides generated by PI3K activity trigger activation of Akt kinases through direct binding to the pleckstrin homology domain and the subsequent phosphorylation of Akt at two conserved residues [21]. Hence, activated Akt modulates the function of numerous substrates involved in the regulation of cell survival, cell cycle progression and cellular growth [22]. Additionally, this pathway may decisively contribute in enabling cancer cells becoming resistant and even more aggressive [23]. These findings, and the fact that PI3K and Akt are highly suited for pharmacologic intervention, make that pathway one of the most attractive targets for therapeutic intervention [24]. It is therefore worth noting that INS significantly reduces both PI3K overexpression and Akt activation by inhibiting its phosphorylation, thus confirming previous results obtained in lung cancer cells [25]. Indeed, INS reduced PI3K levels by about 40%, whereas phosphorylated Akt was down-regulated up to the 35% of its basal values (Fig. 1a and b).

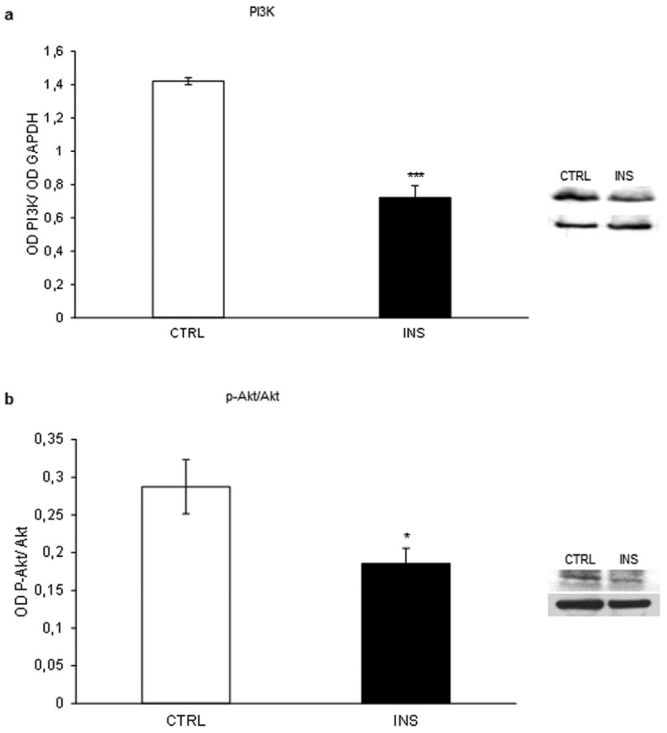

Fig. 1. Immunoblots showing expression of PI3K (a), and p-Akt (b) in MDA-MB-231 cells treated with 4 mM INS for 24 h. Data represent densitometric quantification of optical density (OD) of specific protein signal normalized with the OD values of GAPDH and Akt respectively, used as loading controls. Values are means of three independent experiments, with standard deviations represented by vertical bars. $^{*}p < 0.05$; $^{***}p < 0.001$ by unpaired two-tailed *t*-test.

3.2. Inositol inhibits down-stream effects of Akt activation

MDA-MB-231 breast cancer cells over-expressing active Akt showed prominent mesenchymal features, as down-regulation of E-cadherin, increased expression of molecular signaling components belonging to the NF-kB (COX-2, SNAI1) and Wnt pathways (β-catenin), ultimately leading to β-catenin redistribution in the nucleus, up-regulation of the mesenchymal marker vimentin, and rearrangement of F-actin [26].

E-cadherin down-regulation, often associated with re-expression of N-cadherin, is a pivotal hallmark of EMT [27]. Control cancer cells displayed very low E-cadherin levels, while expressing N-cadherin (Fig. 2a and b). On the contrary, INS treatment restored E-cadherin by increasing seven-fold its levels (Fig. 2b), while only slightly reducing N-cadherin (Fig. 2a).

E-cadherin loss contributes in disassembling E-cadherin/β-catenin complexes, through which cadherin sequesters β-catenin, preventing its dispersion into the cytoplasm, and its subsequent nuclear transcriptional activities [28].

In control cancer cells overall β-catenin is lowered and mostly dispersed around in the cytoplasm. Instead, in INS-treated cells, β-catenin significantly increased by two-fold, while immune staining unveiled a strong signal, mostly located at the cell-to-cell junction level (Fig. 3).

Downward to Akt an orchestrated cascade of molecular events interacts in modulating E-cadherin expression and subsequent transition of the cell from an epithelial toward a mesenchymal phenotype [26]. Meanwhile activation of Wnt pathway is tightly linked to β-catenin modulation, an entrenched cross talk in between COX-2, NF-kB and Notch 1 has been demonstrated cooperatively enhancing expression of SNAI1, a pivotal organizer of EMT [29] and an E-cadherin inhibitor [30]. Indeed, control cells exhibited high intracellular values of those signaling molecules, whereas in INS-treated cells, their concentrations were remarkably reduced. In particular, in INS-treated cells NF-kB and COX-2 decreased by half, while Notch 1 was reduced up to five-fold (Fig. 4). Given that all of these factors positively regulate SNAI1 expression, high SNAI1 levels were observed in control cancer cells while SNAI1 decreased of about 50% after INS addiction (Fig. 4). Ultimately, α-SMA, a specific EMT marker released downstream of the Wnt-pathway activation [31], showed a trend in reduction after INS addiction, even if without reaching statistical significance (Fig. 4).

3.3. Inositol inhibits activation of γ-secretase by downregulating PS1

Increased levels of both Notch 1 and SNAI1 have been reported after activation of presenilin1 (PS1), a key component of the γ-secretase complex. Indeed, PS1 is thought to trigger a complex cascade of molecular events leading to EMT, including E-cadherin down-regulation and Notch-activation (through the release of Notch 1 fragment) [32]. Conversely, PS1 inhibition induces the reversion of EMT molecular features and enhances the responsiveness of cancer cells to chemotherapeutic agents [33]. As we observed a dramatic down-regulation of both Notch 1 and SNAI1 in INS-treated cells, we investigated whether PS1 could also have been influenced by INS administration. As expected, PS1 intracellular levels were down regulated up to three-fold after INS addiction (Fig. 4). This result allows us inferring that reduction in

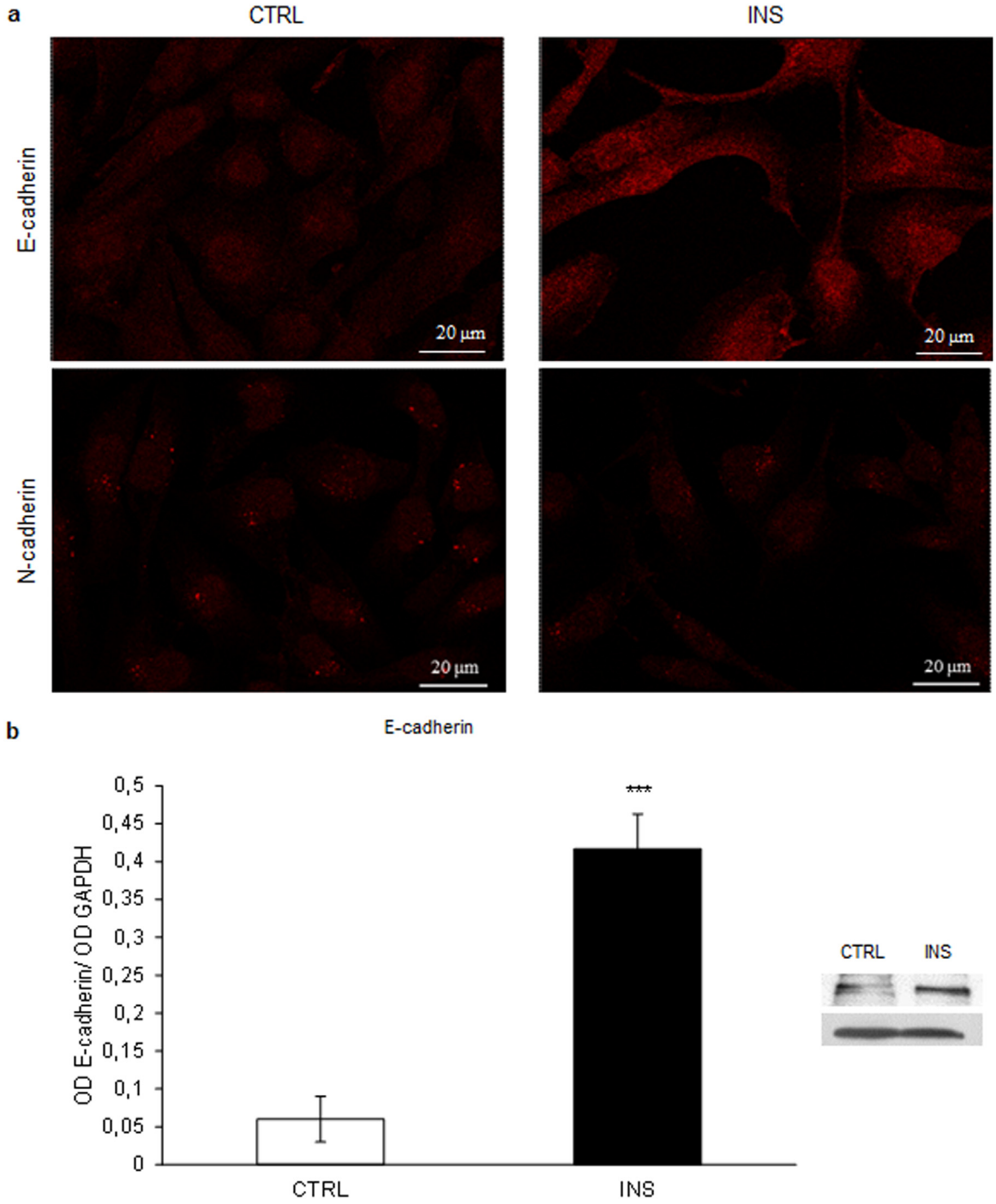

Fig. 2. (a) Confocal microscopy of E-cadherin and N-cadherin distribution in untreated (CTRL) and INS-treated (INS) cells after 24 h. (b) Immunoblots showing expression of E-cadherin in MDA-MB-231 cells treated with 4 mM INS for 24 h. Data represent densitometric quantification of optical density (OD) of specific protein signal normalized with the OD values of GAPDH, used as loading control. Values are means of three independent experiments, with standard deviations represented by vertical bars. $^{***}p < 0.001$ by unpaired two-tailed *t*-test.

Notch 1 and SNAI1 levels may likely to be attributed to PS1 inhibition.

3.4. Inositol inhibits motility and invasiveness of MDA-MB-231 cells

Malignant cells undergoing EMT display increased motility and took advantage of the mesenchymal phenotype acquisition, becoming highly invasive. On the contrary, a noteworthy decrease in invasiveness into MATRIGEL™ was observed in INS-treated cells (Fig. 5a). That behavior is significantly associated to the observed decrease in metalloproteinase-9 (MMP-9) levels after INS treatment (Fig. 5b), while MMP-2 levels were only moderately down-regulated (data not shown). Inhibition of MMP is a key factor in modulation of malignant features, as reduced metalloproteinase activity is likely to hinder the invasiveness competence of cancer cells.

Similarly, results of the wound-healing assay showed that motility performances were also highly impaired in INS-treated breast cancer cells. In control cells, percentage of open area decreased significantly compared to INS-treated breast cancer cells (Fig. 6a and b). Control cells covered the open area within 12 h, leading to an almost complete closure, whereas in INS-treated

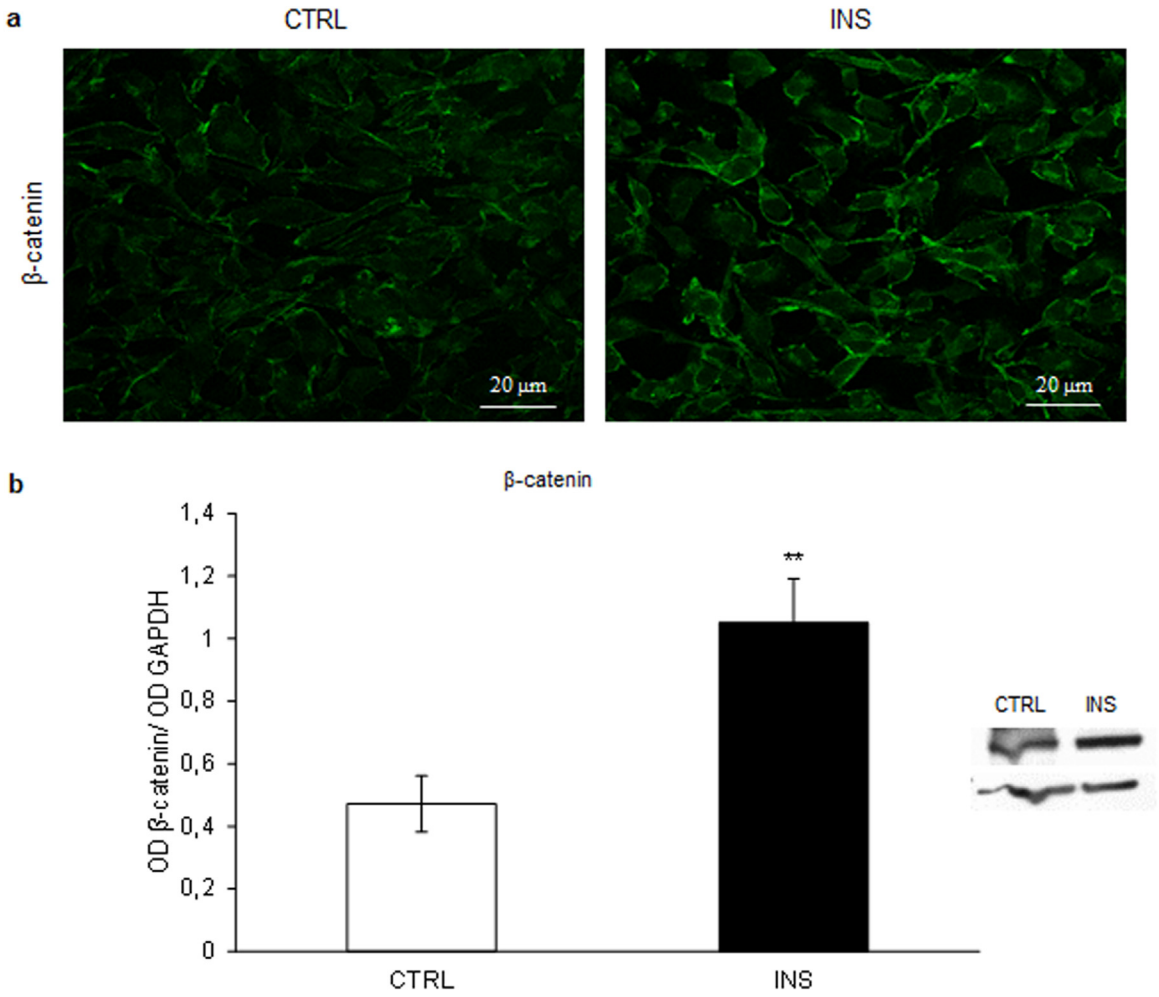

Fig. 3. (a) Confocal microscopy of β-catenin distribution in untreated (CTRL) and INS-treated (INS) cells after 24 h. (b) Immunoblots showing expression of β-catenin in MDA-MB-231 cells treated with 4 mM INS for 24 h. Data represent densitometric quantification of optical density (OD) of specific protein signal normalized with the OD values of GAPDH, used as loading control. Values are means of three independent experiments, with standard deviations represented by vertical bars. $^{**}p < 0.01$ by unpaired two-tailed *t*-test.

cells more than 50% of the area is still open after 12 h. Wound healing results have been confirmed by migration assay, where migrating cells were reduced up to three-fold after INS addition (Fig. 6c). Thereby, INS treatment dramatically reduced both motility and invasiveness of breast cancer cells.

3.5. *Inositol induces cytoskeleton remodeling*

During EMT many cytoskeletal proteins are altered in their expression, localization or activity, thus leading to a profound rearrangement of CSK configuration. Cytoskeleton rearrangement is a mandatory requirement for cells to acquire increased motility/invasiveness properties, and can be considered a remarkable feature belonging to the mesenchymal phenotype.

No significant change in quantitative levels of cytoskeleton proteins (F-actin, vimentin and tubulin) was evidenced by western-blot analysis among controls and treated samples (data not shown). However, when focusing on cancer cells immediately behind the wound healing edge, a meaningful difference emerges regarding F-actin and vimentin behavior.

Indeed, images from confocal microscopy showed that F-actin was differently redistributed in control and in INS-treated cells confined to the wound-healing front. In control cancer cells, F-actin filaments were scattered along the entire cytoplasm, displaying the typical organization belonging to migrating cells. Polarized lamellipodia with treadmilling filaments, as well as filopodia, were clearly observable (Fig. 7a). By contrast, in INS-treated cells stabilized cortical F-actin (SFA) was observed, without any detectable formation of lamellipodia and filopodia. Moreover, in both control and inositol treated cells, stress fibers (SF) were clearly observable, indicating the formation of cell-cell and cell-extracellular matrix (FC) junctional contacts with adhesive behavior (Fig. 7a).

These morphological changes were supported by a quantitative analysis of F-actin, by evaluating the coherency parameter, as previously described [18]. The coherency measure appears to be particularly suited to characterize gradual changes in fibrous textures like the actin cytoskeleton. By its definition, coherency extracts the relative strength of the edges of structures compared to their surroundings and it can therefore be considered “as a measure for detecting the global alterations in the organization of actin cytoskeleton” [18]. Highly invasive cells displayed an unstable cytoskeleton structure, subjected to quick architectural changes, in which likely the inter-filaments connectivity is loosen. As expected, low coherency values were calculated in control metastatic cells, whereas in INS-treated cancer cells coherency significantly increases up to two fold (Fig. 7b).

Lamellipodia are mainly constituted by F-actin filament protruding on the leading edge of the cell, while filopodia are cytoplasmic projections that extend beyond the leading edge of

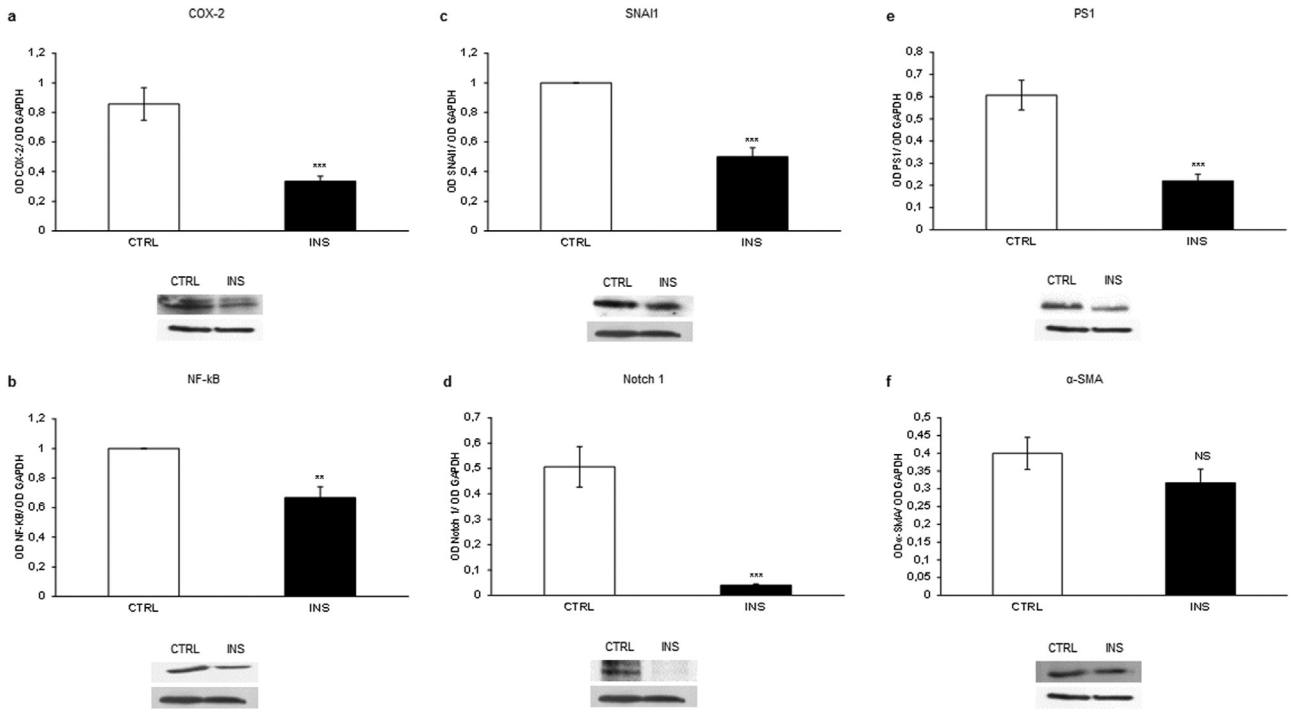

Fig. 4. Immunoblots showing expression of COX-2 (a), NF-kB (b), SNAI1 (c), Notch 1 (d), PS1 (e) and α-SMA (f) in MDA-MB-231 cells treated with 4 mM INS for 24 h. Data represent densitometric quantification of optical density (OD) of specific protein signal normalized with the OD values of GAPDH, used as loading control. Values are means of three independent experiments, with standard deviations represented by vertical bars. $^{**}p < 0.01$; $^{***}p < 0.001$ by unpaired two-tailed *t*-test.

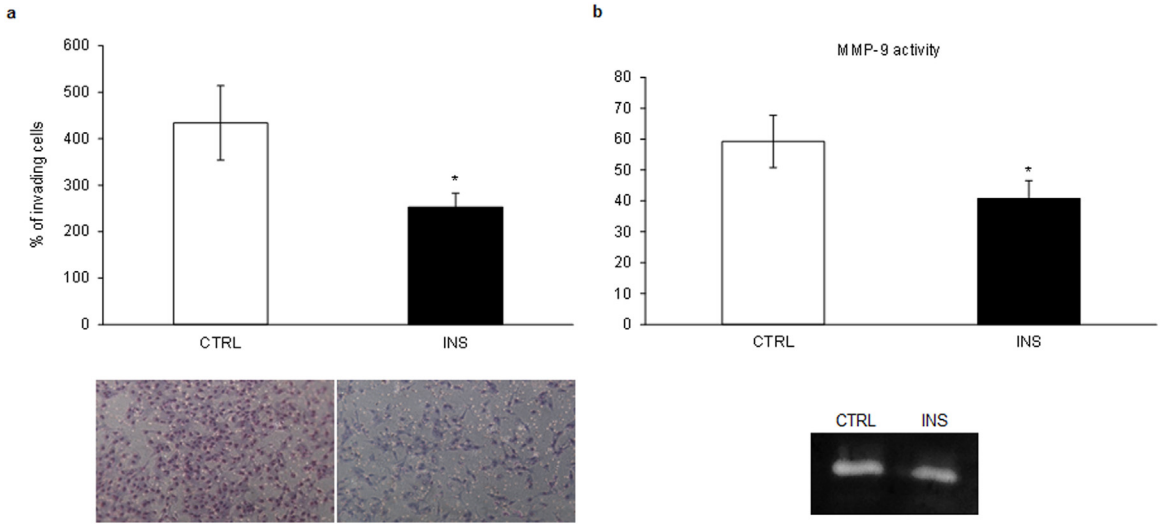

Fig. 5. Effect of INS on invasion (a), and on MMP-9 activity (b) in MDA-MB-231 cells after 24 h. Values are means of three independent experiments, with standard deviations represented by vertical bars. Images were obtained by optical microscopy, with X100 magnification. $^{*}p < 0.05$ by unpaired two-tailed *t*-test.

lamellipodia in migrating cells. They contain actin filaments cross-linked into bundles by actin-binding proteins, like fascin [34].

Fascin is increasingly recognized to play some, even not fully understood, critical functions in cytoskeleton remodeling. Namely, decreased level of fascin correlated with decreased formation of dynamic cell protrusions, decreased proliferation, and reduced invasiveness in cancer cells [35,36].

As expected, we observed a marked decrease in fascin immune staining in INS-treated cells along with the aforementioned sharp decrease in lamellipodia and filopodia (Fig. 8a).

The cofilin pathway has emerged as having a central role in the generation of free actin filament ends resulting in actin filament remodeling by polymerization and depolymerization. Filament remodeling is essential during the formation and retraction of path-finding structures used in the chemotaxis, cell migration and invasion of tumor cells [37]. Cofilin is mainly found in ruffling membranes and at the leading edge of mobile cells, and it is mandatory required in highly migrating cells to ensure cortical contractility [38]. Indeed, high cofilin levels were measured in MDA-MB-231 breast cancer cells, as this protein is required for orchestrating F-actin remodeling in highly migrating cells. On the contrary, in INS-treated cells a dramatic down-regulation of cofilin was observed (Fig. 8b). The above reported distribution pattern of F-actin, fascin and cofilin, provided evidences of cytoskeleton stabilization in INS-treated cells.

The distribution of vimentin in control and INS-treated cells was evaluated by means of confocal microscopy. Vimentin is organized into complex meshwork in control cells as well as in INS-

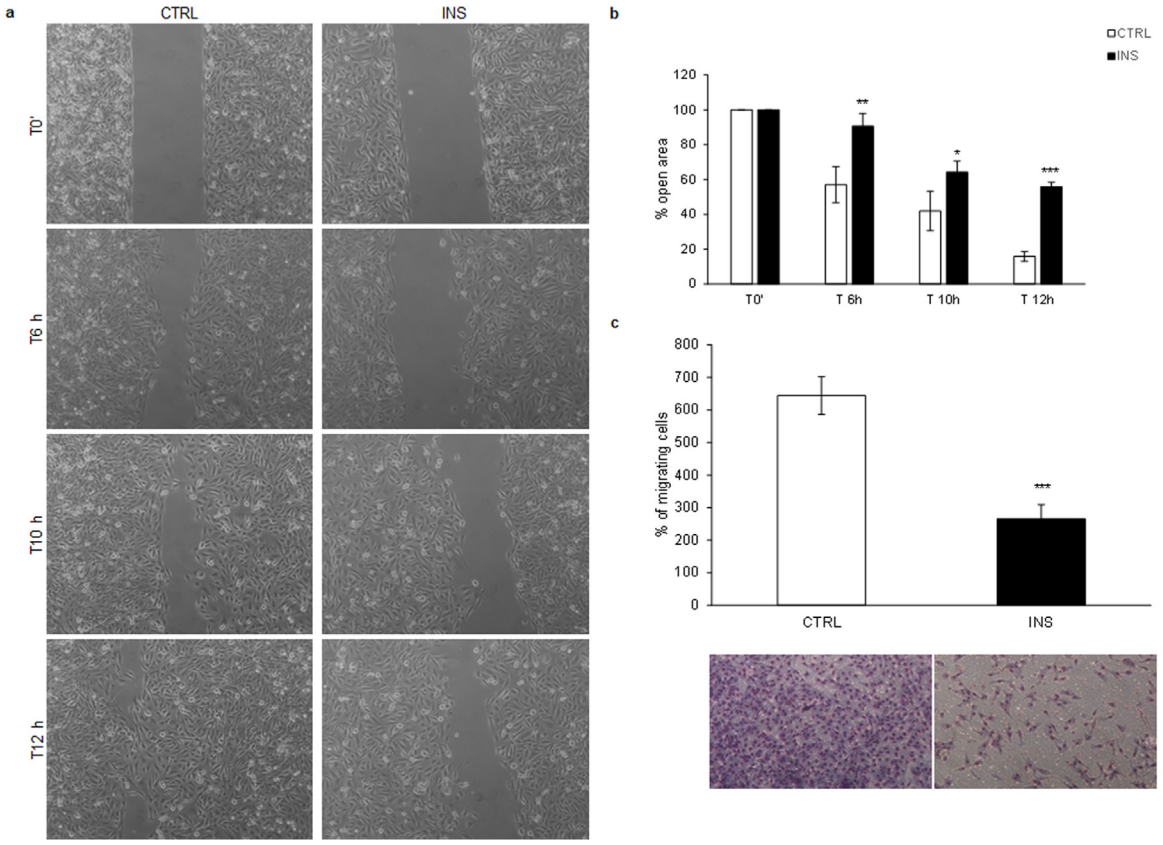

Fig. 6. Effect of INS on wound healing (a, b) and on migration (c) in MDA-MB-231. Values are means of three independent experiments, with standard deviations represented by vertical bars. Images were obtained by optical microscopy, with X100 magnification. $^{*}p < 0.05$; $^{**}p < 0.01$; $^{***}p < 0.001$ by unpaired two-tailed *t*-test.

treated samples, becoming evident in optical sections in which fluorescence intensity of vimentin is maximal (Fig. 9). Yet, an evident decrease in vimentin-related fluorescence intensity was observed in the INS-treated cells distributed along the wound-healing edge, when compared to control cells (Fig. 9a). Furthermore, vimentin showed a peri-nuclear distribution with widespread network of filaments extending towards the cell periphery in control samples. On the contrary, vimentin filaments are scattered along the cytoplasm in INS-treated cells, becoming only partially organized (Fig. 9a).

To assess vimentin quantitative distribution among cells placed behind the wound-healing front, we carried out a quantitative analysis using the Leyca confocal software to determine the maximum amplitude of fluorescence intensity (Sum I) of vimentin both in control and in INS-treated cells.

To obtain a quantitative estimation of vimentin in single cells, the Sum I in a control and in an INS-treated cell, with the same area (2609 μm^2), was evaluated by a confocal software [16]. In the control cell the total amount of fluorescence intensity, expressed as arbitrary unit (a.u.) averaged 1549×10^6 a.u. in the control cell *versus* 522×10^6 a.u. in the INS treated cell. A representative image of vimentin distribution in single cell (both control and treated cells) is shown in Fig. 9b.

Moreover, another study was performed by taking into account 60 optical sections recovered from three different spatial series, in both controls and INS-treated samples. A representative stack profile of seven regions of interest (ROI), randomly drawn along the cytoplasm of a single cell obtained from control and INS-treated samples, is reported in Fig. 9c. Peaks depicted in the diagram (Fig. 9d) indicate fluorescence intensity detected by confocal microscope for each single ROI from the beginning to the end of the sample that is in the total thickness of the examined cell. In INS-treated cells the fluorescence intensity was decreased and the mean value of the maximal amplitude of fluorescence in all ROI analyzed was significantly reduced in respect to the control (CTRL 203.42 a.u. $\pm$ 8.5 *versus* INS 113.1 a.u. $\pm$ 8.5; $p < 0.001$).

To obtain an average estimation of vimentin, about 300 cells for each condition were analyzed. Sum I, significantly decreased in INS-treated cells (CTRL 2.524.437 a.u. $\pm$ 379.388 *versus* INS 947.711 a.u. $\pm$ 234.823; $p < 0.05$).

3.6. Inositol induces changes in quantitative morphometric markers of cell shape

Inositol-treated cancer cells displayed appreciable changes in 2 out of 3 quantitative morphological parameters. Indeed, both Area and solidity were significantly increased (Area: CTRL 1.538 $\mu m^2 \pm 563.4$ *versus* INS 1.800 μm^2 $\pm$ 664.05; $p < 0.001$. Solidity: CTRL 0.13 ± 0.04 *versus* INS 0.17 ± 0.06; $p < 0.001$). Solidity describes in geometrical terms the stiffness and deformability of an object. Thus, the higher the solidity is, the lower the cell deformability. By reducing the cell deformability, in addition with the increase in cell Area we recorded in INS-treated cells, the invasiveness of cancer cells is impaired [17]. On the other hand, roundness was not significantly affected by INS supplementation (data not shown).

3.7. Inositol inhibits cancer cell motility by down-regulating Rock

In mammalian cells, motility control is mostly ruled by the complex dynamics involving Rho-associated protein kinase(s) (Rock 1 and Rock 2). Over-expression of Rock leads to increased motility via enhanced phosphorylation of Myosin Light Chain (PMLC), which is required for actomyosin activity [39,40]. This

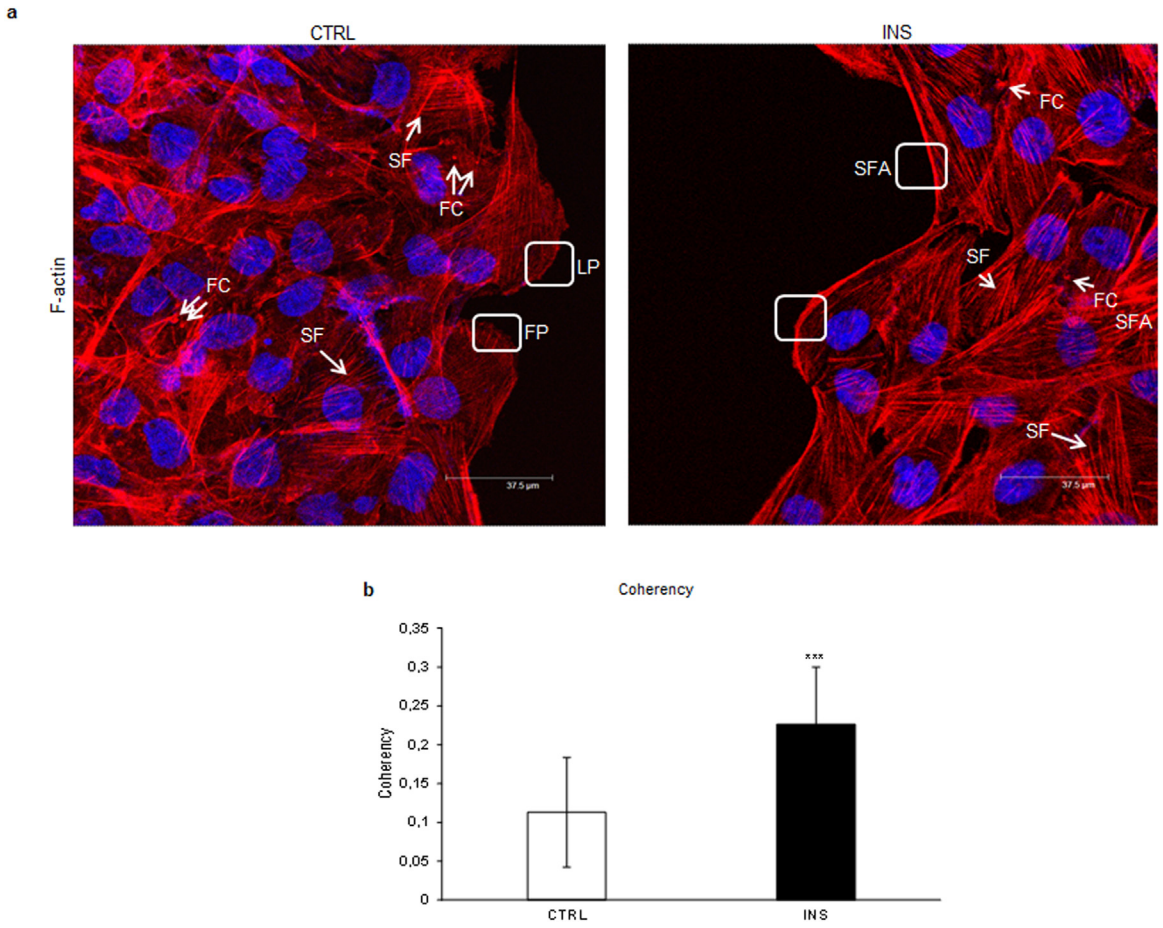

Fig. 7. (a) Confocal microscopy analysis of actin organization in control (CTRL) and INS-treated (INS) cells. Filopodia and lamellipodia are clearly observable in control samples only. LP: lamellipodia, FP: filopodia, SF: stress fibers, FC: focal contacts, SFA: stabilized cortical F-actin. (b) Coherency values per area. Mean and SD were evaluated in randomly chosen images from control sample (n 40) and INS-treated cells (n 40). The equivalent sized regions of interest (ROI) for each experimental condition were analyzed by means of ImageJ v 1.47 h software. Coherency values were calculated as in [18]. $^{***}p < 0.001$ by unpaired two-tailed *t*-test.

pathway is likely to play a very relevant role in conferring migrating and dissemination capabilities to cancer cells, given that inhibition of Rock 1 expression using RNA interference in MDA-MB-231 cells has been shown to significantly impair metastasis [41]. Likewise, targeting Rock 1 pharmacologically abrogates metastasis in animal models [42]. Cancer cells undergoing EMT show high levels of Rock and PMLC [43], as we noticed in MDA-MB-231 cells. However, in INS-treated cells a marked decrease in Rock 1, Rock 2 and, mostly, in PLMC levels was recorded (Fig. 10). Thereby, inhibition of Rock and PMLC, when associated to the aforementioned CSK changes, may help explaining the observed inhibition of motility and invasiveness in INS-treated cells.

3.8. Inositol effects on ZR-75 breast cancer cells

In order to assess INS effects on another metastatic breast cancer cell line, we treated ZR-75 cells with 4 mM INS for 24 h. ZR-75 cells treated with INS showed a significant decrease in key molecular parameters, such as: PS1, NF-kB, COX-2, p-Akt/Akt ratio and fascin in respect to untreated control cells (Fig. 11a–e). Moreover, E-cadherin level remarkably increases (Fig. 11f).

Overall, these data indicated that, even in ZR-75, INS counteracts main EMT molecular features, as such observed in INS-treated MDA-MB-231 cells.

3.9. Inositol physiological concentration only affects PS1 expression both at 24 and at 72 h in MDA-MB-231 cell line

To assess if, in MDA-MB-231 cells, INS physiological concentration (0.1 mM) could give comparable results obtained with the pharmacological dose, we studied key molecular parameters after 24 and 72 h of 0.1 mM INS stimulation.

Both at 24 and at 72 h only PS1 was modulated, by significantly decreasing (Figs. 12a and 13a). NF-kB, COX-2, p-Akt/Akt ratio, fascin and E-cadherin were not significantly affected by 0.1 mM INS stimulation (Figs. 12 and 13).

4. Discussion

Epithelial tumor cells acquire fibroblast-like properties and exhibit increased motility via EMT, which facilitates the escape of tumor cells from primary tumors, therefore fostering the metastatic process [2]. Additionally, EMT contributes in enhancing resistance to conventional chemotherapeutic regimens [3]. Thus, EMT reversion, *i.e.* MET, the inverse process leading a cell to recover an epithelial phenotype, became during the last years a chief therapeutic target.

Herein we observed that MDA-MB-231 breast cancer cells displayed the typical mesenchymal features: low E-cadherin expression and membrane localization of N-cadherin, cytosolic redistribution of β-catenin, enhanced expression of Notch 1, SNAI1 and α-SMA. As expected, these cells showed highly motility and invasive capacity. By adding INS, we such malignant features were

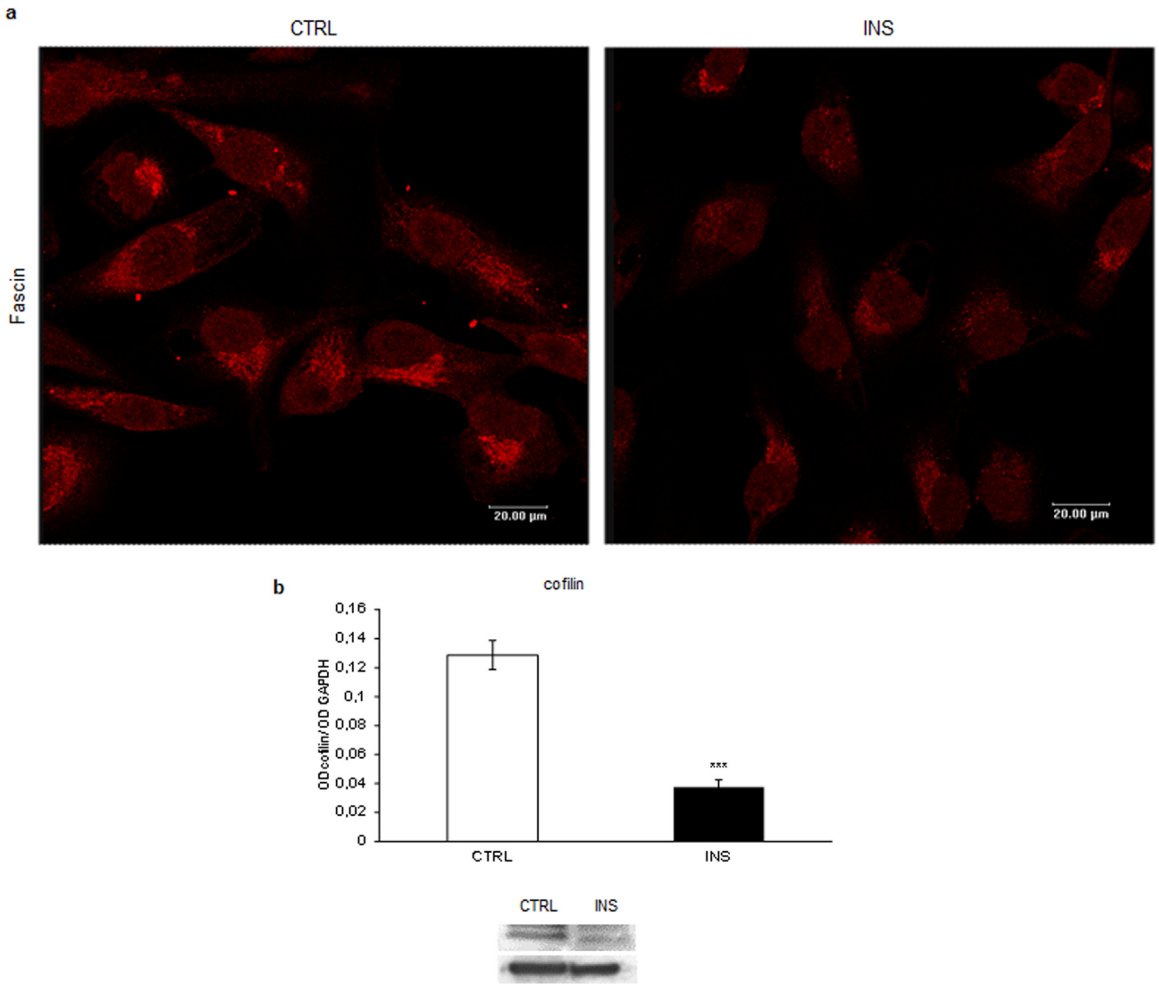

Fig. 8. (a) Confocal microscopy of fascin distribution in untreated (CTRL) and INS-treated cells (INS) after 24 h. (b) Immunoblots showing expression of cofilin in MDA-MB-231 cells treated with 4 mM INS for 24 h. Data represent densitometric quantification of optical density (OD) of specific protein signal normalized with the OD values of GAPDH, used as loading control. Values are means of three independent experiments, with standard deviations represented by vertical bars. $^{***}p < 0.001$ by unpaired two-tailed *t*-test.

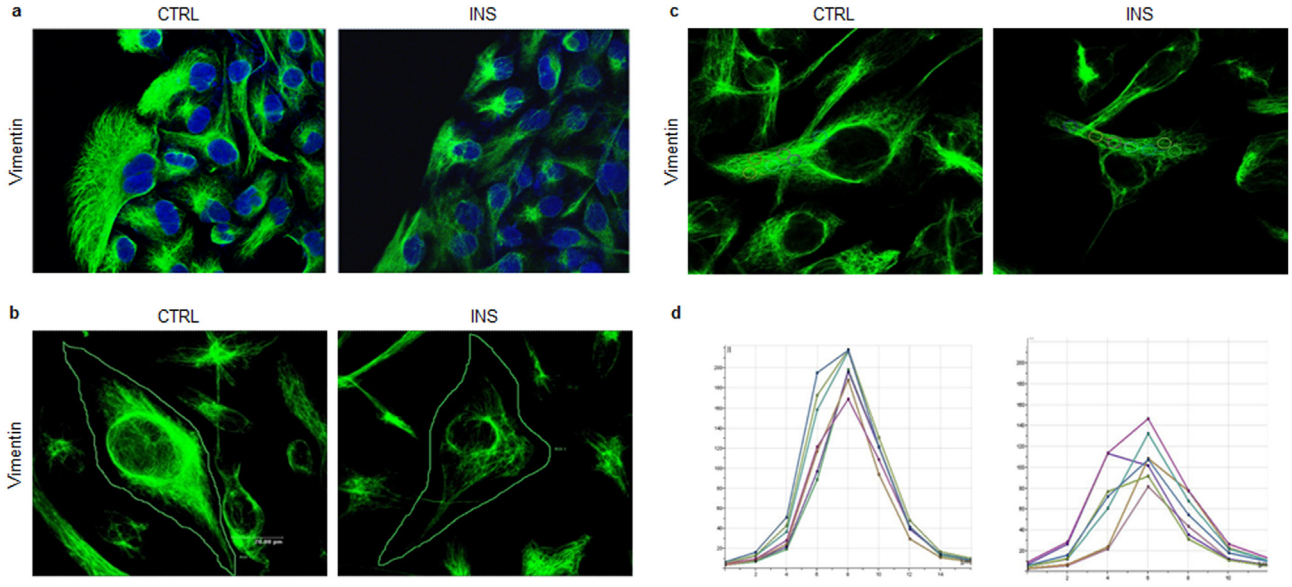

Fig. 9. (a) Confocal microscopy of vimentin distribution in untreated (CTRL) and INS-treated cells (INS) after 24 h. (b) Representative single cell images of vimentin fluorescence intensity in untreated (CTRL) and INS-treated cells (INS) after 24 h. Values of fluorescence intensity are reported in the text. (c) Representative stack profile of seven regions of interest (ROI) randomly drawn in cytoplasm of untreated (CTRL) and INS-treated (INS) cells. (d) Vimentin fluorescence intensity measured in ROI from both untreated (CTRL) and INS-treated (INS) cells. Fluorescence distribution is plotted against the z position of the optical section, leading to a curve with different intensity peaks, spanning from the beginning to the end of the series. *Y*-axis: fluorescence intensity. *X*-axis: z position of the optical section.

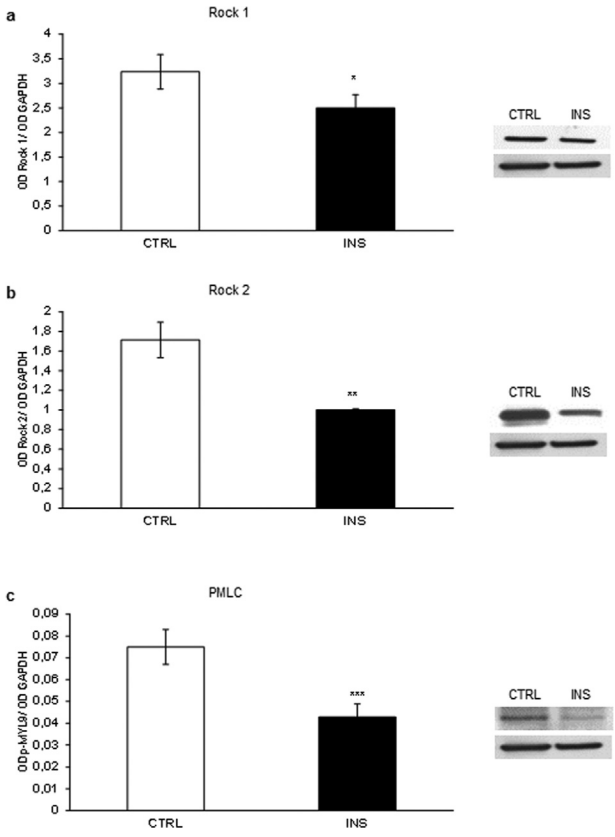

Fig. 10. Immunoblots showing expression of Rock 1 (a), Rock 2 (b) and PMLC (c) in MDA-MB-231 cells treated with 4 mM INS for 24 h. Data represent densitometric quantification of optical density (OD) of specific protein signal normalized with the OD values of GAPDH, used as loading control. Values are means of three independent experiments, with standard deviations represented by vertical bars. $^{*}p < 0.5$; $^{**}p < 0.01$; $^{***}p < 0.001$ by unpaired two-tailed *t*-test.

almost completely suppressed. Indeed, INS-treated MDA-MB-231 cells re-expressed E-cadherin, lost N-cadherin and showed an increased redistribution of β-catenin behind cell membrane, while both motility and invading capacity were severely inhibited. These changes were associated with a significant down-regulation of PI3K/Akt activity that likely led to a further decrease in downstream signaling effectors: NF-kB, COX-2, and SNAI1. Inhibition of PS1 further contributed in decreasing SNAI1 levels by lowering Notch 1 release. Overall, these data indicated that INS inhibits the principal molecular pathway supporting the epithelial-mesenchymal transition.

These key molecular events were also confirmed in the metastatic breast cancer cell line ZR-75. After INS addition, p-Akt/Akt ratio, COX-2, NF-kB, PS1 and fascin were significantly down regulated, whereas E-cadherin expression was up regulated.

These biochemical changes were mirrored by the associated modifications observed on cytoskeleton components. INS significantly reduces vimentin expression in cells behind the wound-healing edge and stabilizes cortical F-actin.

Furthermore, lamellipodia and filopodia, two specific membrane extensions enabling both cell migration and invasiveness, were no longer detectable in INS-treated samples, meanwhile fascin and cofilin were highly reduced. As these modifications were especially evident at the edge of the motility front, it can be surmised that INS-induced CSK changes may significantly contribute in stabilizing cell structure and suppressing motility and invasiveness. Such conclusion is further confirmed by the results of the quantitative analysis of both cell shape and F-actin coherency. Indeed, INS-treated MDA-MB-231 breast cancer cells displayed a stable, 'solid' phenotype, characterized by a more ordered cytoskeleton configuration as suggested by the high coherency values of F-actin network.

Inositol and its derivatives are a family of highly phylogenetically conserved polyols that stabilizes proteins and cytoskeleton architecture in cells exposed to environmental and chemical stress [44]. The chemistry and biology of inositols, and its phosphorylated derivatives, have become intense areas of research during the last two decades due to their involvement in various cellular signaling processes [45]. Namely, inositol-hexakisphosphate (phytate, IP6) and inositol have been demonstrated to exert a wide array of anticancer effects, presumably through a multi-targeted activity, both *in vitro* [46] as well as *in vivo* [47]. Inositol has been proven to inhibit the PI3K/Akt pathway in cancer and to participate in CSK remodeling. As the activation of PI3K/Akt axis is emerging as a pivotal feature of EMT [6], altogether with CSK remodeling, we hypothesize that myo-inositol addiction could revert that transition in breast cancer cells in which inositol has previously been demonstrated to be effective [47]. Indeed, data obtained by our experimental model supported this hypothesis and indicated that myo-inositol is successful in inducing MET in MDA-MB-231 cells. It has been previously evidenced that re-expression of full-length E-cadherin is sufficient in MDA-MB-231 cells to restore a morphological and functional reversion of the epithelial phenotype [48]. Thereby it is likely that INS, in re-expressing E-cadherin up to seven fold when compared with control cells, may trigger MET thought that pathway. Inhibition of both migrating capability and invasiveness are indeed compatible with the reversion of the mesenchymal phenotype, even if such transition cannot be considered 'complete'. In fact, INS does not slow-down α-SMA in a significant manner, even if an undisputed trend in α-SMA reduction was observed. Different MET subtypes – as opposed to 'complete' MET – have been described, comprising a wide spectrum of changes in epithelial plasticity [49,50]. Therefore, it can be hypothesized that INS contributes in triggering MET, yet without achieving a 'full', complete transition. Nevertheless, even if pharmacological dose of INS displays an efficient activity on several, different molecular targets, yet some redundant pathways may be still active in maintaining a few EMT features. Moreover, such effects are observed only with the pharmacological concentration of INS, as that utilized in clinical settings [12]. Physiological values of INS in blood range from 0.03 to 0.1 mM [51]. At the used physiological concentration (0.1 mM), no significant changes were recorded in our experiments. Noticeably, the only exception was represented by the meaningful decrease in PS1 levels, observed at both 24 and 72 h. This result is intriguing as it suggests that INS exerts an inhibitory control on PS1 activity under physiological conditions.

Results provided herein should be considered as a preliminary hint, which deserves further studies to identify the mechanistic details supporting the INS-based activity on cancer cells. As the restoration of a MET program should efficiently slow down the differentiation and dissemination of cancer cells, such results may be of interest, as targeting EMT processes is becoming a relevant issue in tumor management.

Acknowledgment

Abdel Halim Harrath, Saleh H. Alwasel and Mariano Bizzarri would like to extend their sincere appreciation to the Deanship of Scientific Research at King Saud University (Saudi Arabia) for funding this Research group No. (RG#164).

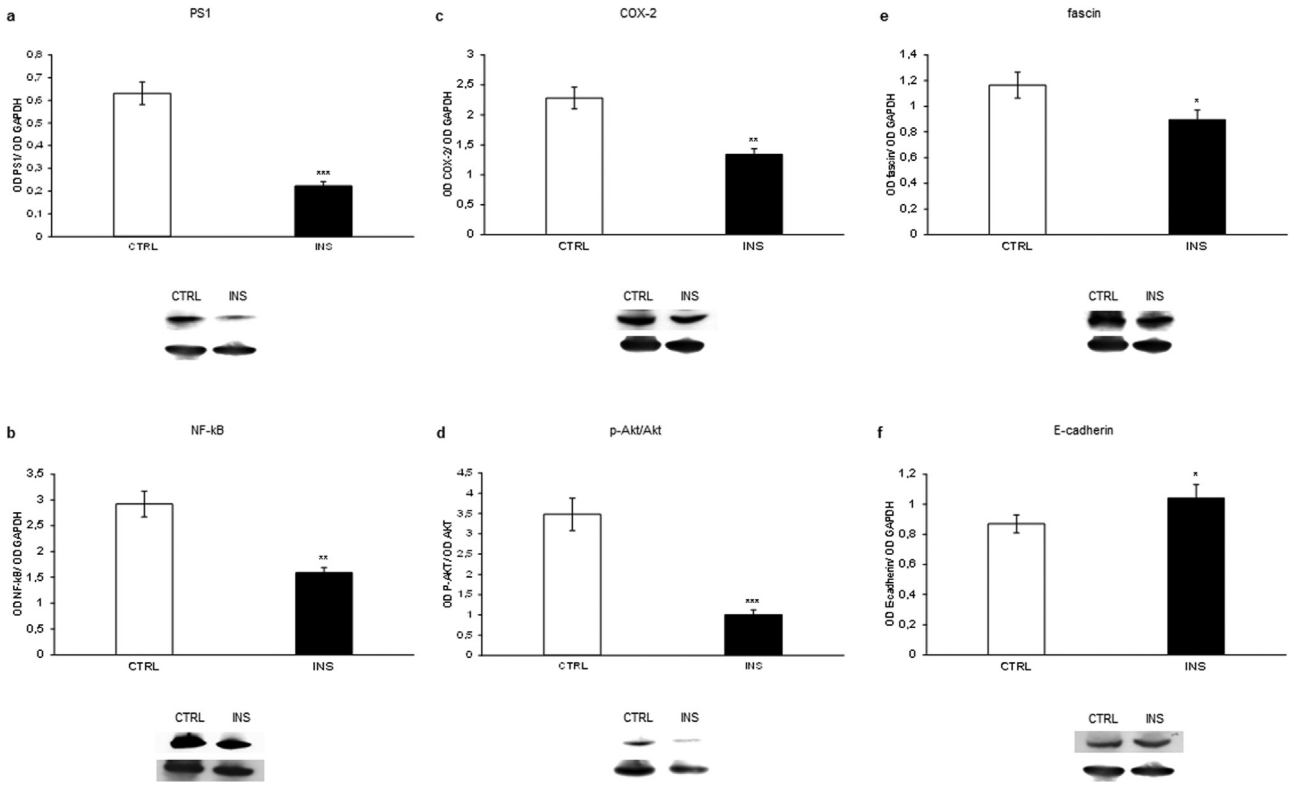

Fig. 11. Immunoblots showing expression of PS1 (a), NF-kB (b), COX-2 (c), p-Akt/Akt ratio (d), fascin (e), E-cadherin (f) in ZR-75 cells treated with 4 mM INS for 24 h. Data represent densitometric quantification of optical density (OD) of specific protein signal normalized with the OD values of GAPDH as loading control; p-Akt was normalized using Akt as loading control. Values are means of three independent experiments, with standard deviations represented by vertical bars. $^{*}p < 0.5$; $^{**}p < 0.01$; $^{***}p < 0.001$ by unpaired two-tailed *t*-test.

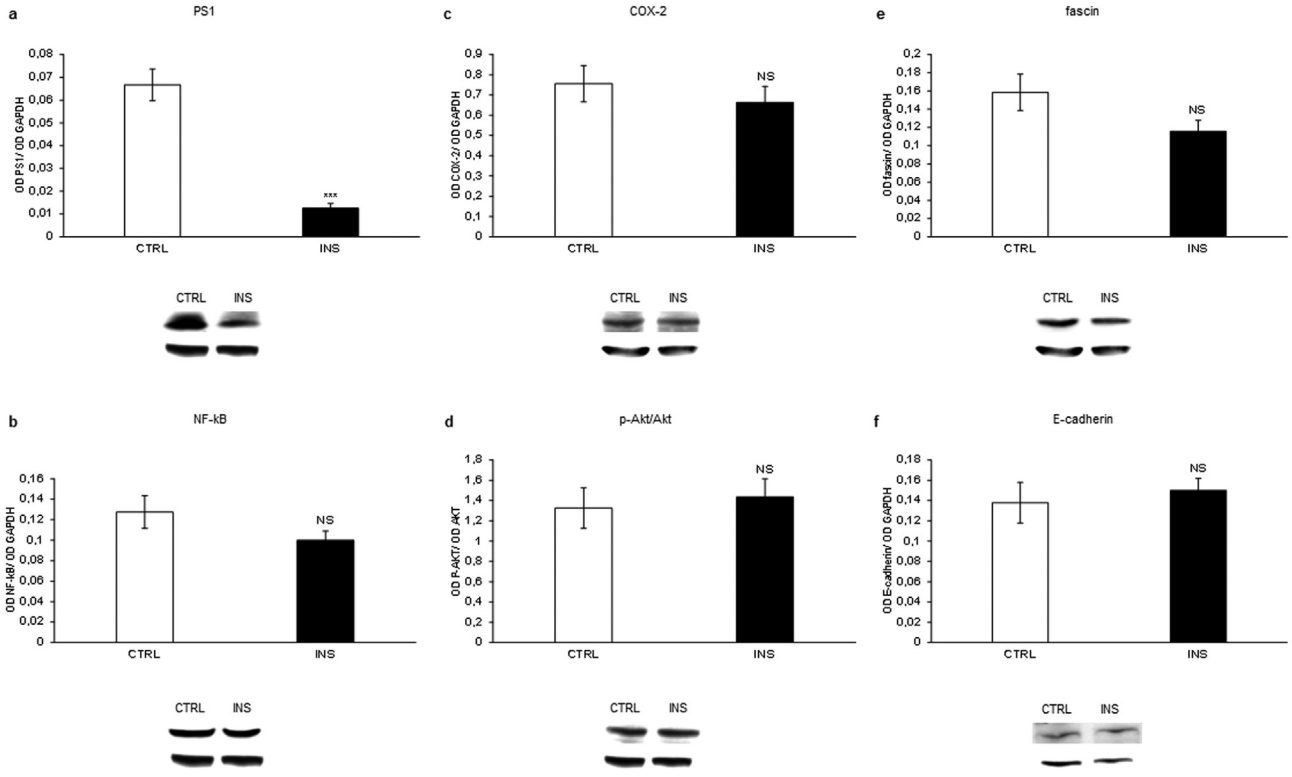

Fig. 12. Immunoblots showing expression of PS1 (a), NF-kB (b), COX-2 (c), p-Akt/Akt ratio (d), fascin (e), E-cadherin (f) in MDA-MB-231 cells treated with 0.1 mM INS for 24 h. Data represent densitometric quantification of optical density (OD) of specific protein signal normalized with the OD values of GAPDH as loading control; p-Akt was normalized using Akt as loading control. Values are means of three independent experiments, with standard deviations represented by vertical bars. $^{***}p < 0.001$ by unpaired two-tailed *t*-test.

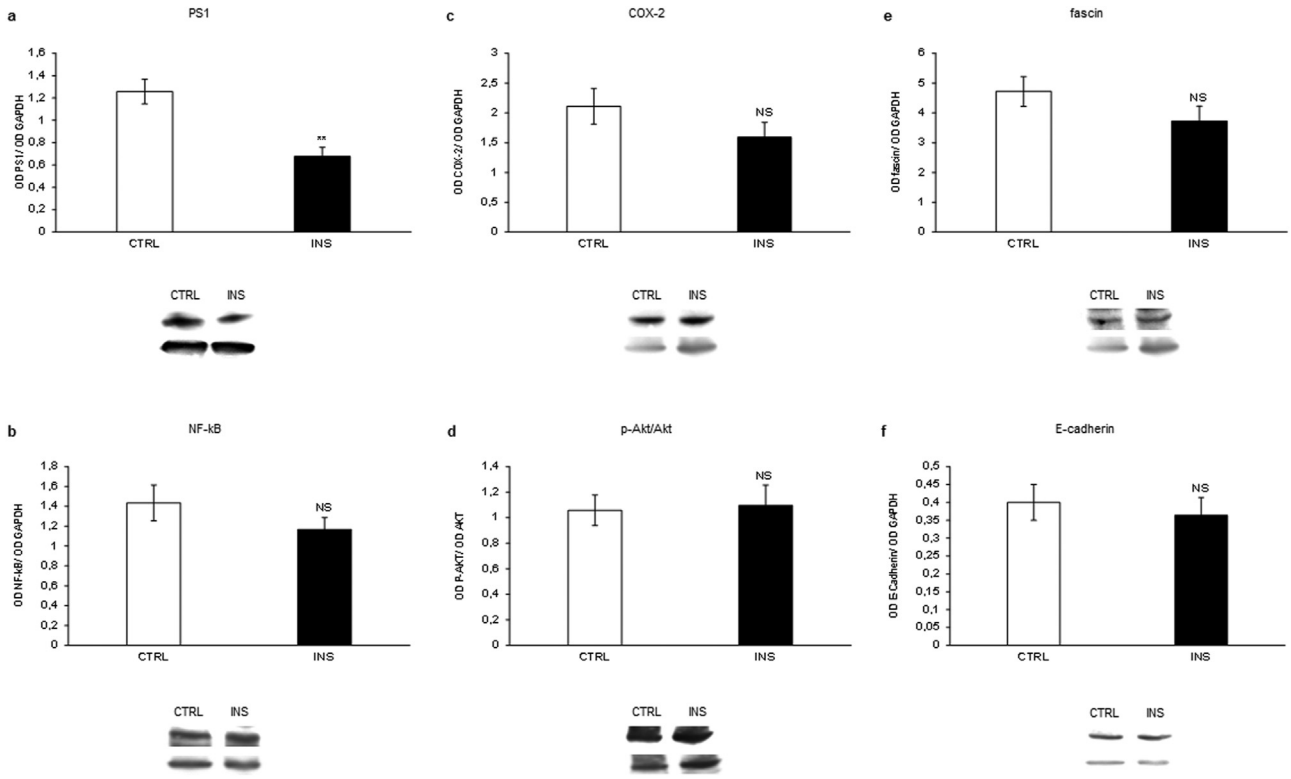

Fig. 13. Immunoblots showing expression of PS1 (a), NF-kB (b), COX-2 (c), p-Akt/Akt ratio (d), fascin (e), E-cadherin (f) in MDA-MB-231 cells treated with 0.1 mM INS for 72 h. Data represent densitometric quantification of optical density (OD) of specific protein signal normalized with the OD values of GAPDH as loading control; p-Akt was normalized using Akt as loading control. Values are means of three independent experiments, with standard deviations represented by vertical bars. $^{**}p < 0.01$ by unpaired two-tailed *t*-test.

Disclosures

The authors declare no conflict of interest.

References

[1] J.P. Thiery, Epithelial-mesenchymal transitions in development and pathologies, Curr. Opin. Cell Biol. 15 (2003) 740–746.
[2] J.P. Thiery, Epithelial-mesenchymal transitions in tumour progression, Nat. Rev. Cancer 2 (2002) 442–454.
[3] S. Hiscox, L. Morgan, D. Barrow, C. Dutkowskil, A. Wakeling, R.I. Nicholson, Tamoxifen resistance in breast cancer cells is accompanied by an enhanced motile and invasive phenotype: inhibition by gefitinib ('Iressa', ZD1839), Clin. Exp. Metastasis 21 (2004) 201–212.
[4] N.K. Kurrey, S.P. Jalgaonkar, A.V. Joglekar, A.D. Ghanate, P.D. Chaskar, R. Y. Doiphode, S.A. Bapat, Snail and slug mediate radioresistance and chemoresistance by antagonizing p53-mediated apoptosis and acquiring a stem-like phenotype in ovarian cancer cells, Stem Cells 27 (2009) 2059–2068.
[5] J.P. Thiery, J.P. Sleeman, Complex networks orchestrate epithelial mesenchymal transitions, Nat. Rev. Mol. Cell Biol. 7 (2006) 131–142.
[6] D. Yao, C. Dai, S. Peng, Mechanism of the mesenchymal–epithelial transition and its relationship with metastatic tumor formation, Mol. Cancer Res. 9 (2011) 1608–1620.
[7] H. Acloque, M.S. Adams, K. Fishwick, M. Bronner-Fraser, M.A. Nieto, Epithelial-mesenchymal transitions: the importance of changing cell state in development and disease, J. Clin. Investig. 119 (2009) 1438–1449.
[8] K.R. Ginnebaugh, A. Ahmad, F.H. Sarkar, The therapeutic potential of targeting the epithelial–mesenchymal transition in cancer, Expert Opin. Ther. Target 18 (2014) 731–745.
[9] C.P. Downes, The cellular function of myo-inositol, Biochem. Soc. Trans. 17 (1989) 259–268.
[10] M.T. Kane, M. Norris, P.A. Harrison, Uptake and incorporation of inositol by preimplantation mouse embryos, J. Reprod. Fertil. 96 (1992) 617–625.
[11] J. Larner, D-chiro-inositol–its functional role in insulin action and its deficit in insulin resistance, Int. J. Exp. Diabetes Res. 3 (2002) 47–60.
[12] S. Dinicola, T.T. Chiu, V. Unfer, G. Carlomagno, M. Bizzarri, The rationale of the myo-inositol and D-chiro-inositol combined treatment for polycystic ovary syndrome, J. Clin. Pharmacol. 54 (2014) 1079–1092.
[13] I. Vucenik, A.M. Shamsuddin, Cancer inhibition by inositol hexaphosphate (IP6) and inositol: from laboratory to clinic, J. Nutr. 133 (Suppl 1) (2003) 3778S–3784S.
[14] C. Huang, N.C. Liang, Increase in cytoskeletal actin induced by inositol 1,4-bisphosphate in saponin-permeated pig platelets, Cell Biol. Int. 18 (1994) 797–804.
[15] T. Suzuki, H. Hara, Phytate hydrolysate induces circumferential F-actin ring formation at cell-cell contacts by a Rho-associated kinase dependent mechanism in colorectal cancer HT-29 cells, Mol. Nutr. Food Res. 54 (2010) 1807–1818.
[16] F. Ferranti, M. Caruso, M. Cammarota, M.G. Masiello, K. Corano Scheri, C. Fabrizi, L. Fumagalli, C. Schiraldi, A. Cucina, A. Catizone, G. Ricci, Cytoskeleton modifications and autophagy induction in TCam-2 seminoma cells exposed to simulated microgravity, Biomed. Res. Int. 2014 (2014) 904396.
[17] A. Pasqualato, V. Lei, A. Cucina, S. Dinicola, F. D'Anselmi, S. Proietti, M. G. Masiello, A. Palombo, M. Bizzarri, Shape in migration: quantitative image analysis of migrating chemoresistant HCT-8 colon cancer cells, Cell Adhes. Migr. 7 (2013) 450–459.
[18] J. Weichsel, N. Herold, M.J. Lehmann, H.G. Kräusslich, U.S. Schwarz, A quantitative measure for alterations in the actin cytoskeleton investigated with automated high-throughput microscopy, Cytometry A 77 (2010) 52–63.
[19] Z. Püspöki, M. Storath, D. Sage, M. Unser, Transforms and Operators for Directional bioimage Analysis: A Survey, ⟨https://pdfs.semanticscholar.org/78e2/6c10a0316db7a9f0a90f3bd8823665090a1d.pdf⟩.
[20] A.M. Gustafson, R. Soldi, C. Anderlind, M.B. Scholand, J. Qian, X. Zhang, K. Cooper, D. Walker, A. McWilliams, G. Liu, E. Szabo, J. Brody, P.P. Massion, M. E. Lenburg, S. Lam, A.H. Bild, A. Spira, Airway PI3K pathway activation is an early and reversible event in lung cancer development, Sci. Transl. Med. 2 (2010) 26ra25.
[21] J.R. Woodgett, Recent advances in the protein kinase B signaling pathway, Curr. Opin. Cell Biol. 17 (2005) 150–157.
[22] J.A. Fresno Vara, E. Casado, J. de Castro, P. Cejas, C. Belda-Iniesta, M. González-Barón, PI3K/Akt signalling pathway and cancer, Cancer Treat. Rev. 30 (2004) 193–204.
[23] J. Lim, J.H. Kim, J.Y. Paeng, M.J. Kim, S.D. Hong, J.I. Lee, S.P. Hong, Prognostic value of activated Akt expression in oral squamous cell carcinoma, J. Clin. Pathol. 58 (2005) 1199–1205.
[24] B.T. Hennessy, D.L. Smith, P.T. Ram, Y. Lu, G.B. Mills, Exploiting the PI3K/AKT pathway for cancer drug discovery, Nat. Rev. Drug Discov. 4 (2005) 988–1004.
[25] W. Han, J.J. Gills, R.M. Memmott, S. Lam, P.A. Dennis, The chemopreventive agent myoinositol inhibits Akt and extracellular signal-regulated kinase in bronchial lesions from heavy smokers, Cancer Prev. Res. 2 (2009) 370–376.
[26] S.J. Grille, A. Bellacosa, J. Upson, A.J. Klein-Szanto, F. van Roy, W. Lee-Kwon, M. Donowitz, P.N. Tsichlis, L. Larue, The protein kinase Akt induces epithelial-mesenchymal transition and promotes enhanced motility and invasiveness of

squamous cell carcinoma lines, Cancer Res. 63 (2003) 2172–2178.
[27] H. Peinado, F. Portillo, A. Cano, Transcriptional regulation of cadherins during development and carcinogenesis, Int. J. Dev. Biol. 48 (2004) 365–375.
[28] S. Orsulic, O. Huber, H. Aberle, S. Arnold, R. Kemler, E-cadherin binding prevents beta-catenin nuclear localization and beta-catenin/LEF-1- mediated transactivation, J. Cell Sci. 112 (1999) 1237–1245.
[29] D. Medici, E.D. Hay, B.R. Olsen, Snail and Slug promote epithelial-mesenchymal transition through beta-catenin-T-cell factor-4-dependent expression of transforming growth factor-beta3, Mol. Biol. Cell 19 (2008) 4875–4887.
[30] J.R. Graff, J.G. Herman, R.G. Lapidus, H. Chopra, R. Xu, D.F. Jarrard, W.B. Isaacs, P. M. Pitha, N.E. Davidson, S.B. Baylin, E-cadherin expression is silenced by DNA hypermethylation in human breast and prostate carcinomas, Cancer Res. 55 (1995) 5195–5199.
[31] G. Serini, M.L. Bochaton-Piallat, P. Ropraz, A. Geinoz, L. Borsi, L. Zardi, G. Gabbiani, The fibronectin domain ED-A is crucial for myofibroblastic phenotype induction by transforming growth factor-1, J. Cell. Biol., 142, (1998) 873–881.
[32] M.E. Fortini, Gamma-secretase-mediated proteolysis in cell-surface-receptor signaling, Nat. Rev. Mol. Cell Biol. 3 (2002) 673–684.
[33] J. Han, Q. Shen, Targeting γ-secretase in breast cancer, Breast Cancer Target Ther. 4 (2012) 83–90.
[34] C. Le Clainche, M.F. Carlier, Regulation of actin assembly associated with protrusion and adhesion in cell migration, Physiol. Rev. 88 (2008) 489–513.
[35] J.J. Xie, L.Y. Xu, H.H. Zhang, W.J. Cai, R.Q. Mai, Y.M. Xie, Z.M. Yang, Y.D. Niu, Z. Y. Shen, E.M. Li, Role of fascin in the proliferation and invasiveness of esophageal carcinoma cells, Biochem. Biophys. Res. Commun. 337 (2005) 355–362.
[36] Y. Hashimoto, M. Skacel, J.C. Adams, Roles of fascin in human carcinoma motility and signaling: prospects for a novel biomarker? Int. J. Biochem. Cell Biol. 37 (2005) 1787–1804.
[37] P. Lappalainen, D.G. Drubin, Cofilin promotes rapid actin filament turnover *in vivo*, Nature 388 (1997) 78–82.
[38] M.F. Carlier, V. Laurent, J. Santolini, R. Melki, D. Didry, G.X. Xia, Y. Hong, N. H. Chua, D. Pantaloni, Actin depolymerizing factor (ADF/cofilin) enhances the rate of filament turnover: implication in actin-based motility, J. Cell Biol. 136 (1997) 1307–1322.
[39] D.M. Gilkes, L. Xiang, S.J. Lee, P. Chaturvedi, M.E. Hubbi, D. Wirtz, G.L. Semenza, Hypoxia-inducible factors mediate coordinated RhoA-ROCK1 expression and signaling in breast cancercells, Proc. Natl. Acad. Sci. USA 111 (2014) E384–E393.
[40] J.B. Wyckoff, S.E. Pinner, S. Gschmeissner, J.S. Condeelis, E. Sahai, ROCK- and myosin-dependent matrix deformation enables protease-independent tumor-cell invasion *in vivo*, Curr. Biol. 16 (2006) 1515–1523.
[41] S. Liu, R.H. Goldstein, E.M. Scepansky, M. Rosenblatt, Inhibition of rho-associated kinase signaling prevents breast cancer metastasis to human bone, Cancer Res. 69 (2009) 8742–8751.
[42] K. Itoh, K. Yoshioka, H. Akedo, M. Uehata, T. Ishizaki, S. Narumiya, An essential part for Rho-associated kinase in the transcellular invasion of tumor cells, Nat. Med. 5 (1999) 221–225.
[43] A.R. Horwitz, J.T. Parsons, Cell migration: movin' on, Science 286 (1999) 1102–1103.
[44] R.H. Michell, Inositol derivatives: evolution and functions, Nat. Rev. Mol. Cell Biol. 9 (2008) 151–161.
[45] W. Chen, Z. Deng, K. Chen, D. Dou, F. Song, L. Li, Z. Xi, Synthesis and *in vitro* anticancer activity evaluation of novel bioreversible phosphate inositol derivatives, Eur. J. Med. Chem. 93 (2015) 172–181.
[46] A.K.M. Shamsuddin, I. Vucenik, IP6 and inositol in cancer prevention and therapy, Curr. Cancer Ther. Rev. 1 (2005) 259–269.
[47] I. Bacić, N. Druzijanić, R. Karlo, I. Skifić, S. Jagić, Efficacy of IP6+ inositol in the treatment of breast cancer patients receiving chemotherapy: prospective, randomized, pilot clinical study, J. Exp. Clin. Cancer Res. 29 (2010) 12.
[48] Y.L. Chao, C.R. Shepard, A. Wells, Breast carcinoma cells re-express E-cadherin during mesenchymal to epithelial reverting transition, Mol. Cancer 9 (2010) 179.
[49] A. Eger, W. Mikulits, Models of epithelial-mesenchymal transition, Drug Discov. Today Dis. Model 2 (2005) 57–63.
[50] S. Grünert, M. Jechlinger, H. Beug, Diverse cellular and molecular mechanisms contribute to epithelial plasticity and metastasis, Nat. Rev. Mol. Cell Biol. 4 (2003) 657–665.
[51] B.J. Holub, Nutritional, biochemical, and clinical aspects of inositol and phosphatidylinositol metabolism, Can. J. Physiol. Pharmacol. 62 (1984) 1–8.